Pressure Drop and Mass Transfer in Two-Pass Ribbed Channels

P. R. Chandra* and J. C. Han†
Texas A&M University, College Station, Texas

The combined effects of the sharp 180-deg turn and of the rib configuration on the pressure drop and mass transfer characteristics in a two-pass square channel with a pair of opposite rib-roughened walls (to simulate turbine airfoil cooling passages) were determined for a Reynolds number range of 10,000–60,000. For pressure drop experiments, the rib height-to-hydraulic diameter ratios e/D were 0.063 and 0.094; the rib pitch-to-height ratios P/e were 10 and 20; the rib angles-of-attack α were 90, 60, and 45 deg. For mass transfer experiments, the top, bottom, inner, and outer walls of the test channel were naphthalene-coated surfaces; the e/D ratio was 0.063; the P/e ratio was 10; the α was 90 or 60 deg. Heat transfer enhancements were compared for the first pass and for the two-pass channel with the sharp 180-deg turn. Correlations for the fully-developed friction factors and loss coefficients were obtained.

Nomenclature

D = channel width; also, hydraulic diameter
e = rib height
e^+ = roughness Reynolds number $= (e/D)Re(f/2)^{1/2}$
$\bar{f}$ = average friction factor in a channel with two opposite ribbed walls
$\bar{f}_{bt}$ = average friction factor in the fully developed before-turn region
$\bar{f}_{at}$ = average friction factor in the fully developed after-turn region
f_o = fully developed smooth tube friction factor
G = air mass velocity $= \rho v$
g_c = conversion factor
h_m = local mass transfer coefficient
K_c = loss coefficient due to sudden contraction at the entrance
K_t = loss coefficient for the sharp 180° turn
ΔL = channel length for fully developed pressure drop
M = cumulative mass transferred
$\dot{m}$ = local mass transfer rate per unit area
Nu = Nusselt number $= hD/K$
Nu_o = fully developed smooth tube Nusselt number
ΔP = pressure drop
P = rib pitch
P_i = pressure at channel entrance
P_x = pressure at axial distance from channel entrance
Pr = Prandtl number of air
Re = Reynolds number based on channel hydraulic diameter, GD/μ
Sc = Schmidt number for naphthalene
Sh = local Sherwood number
Sh_o = fully developed smooth tube Sherwood number
Sh_r = the rib-side-wall Sherwood number
$\bar{Sh}_r$ = the rib-side-wall average Sherwood number
St = Stanton number $= Nu/(RePr)$
$\bar{St}_r$ = the ribbed-side-wall average Stanton number
St_o = fully developed smooth tube Stanton number
Δt = duration of the test run
v = air velocity
X = axial distance from channel entrance
$\tilde{D}$ = diffusion coefficient
α = rib angle-of-attack
ρ_b = bulk naphthalene vapor density
ρ_s = solid naphthalene density
ρ_w = local naphthalene vapor density at wall
ν = kinematic viscosity of pure air $= \mu/\rho$

Received March 10, 1988; revision received Sept. 6, 1988.

*Graduate Assistant; currently Assistant Professor, Department of Mechanical Engineering, McNeese State University, Lake Charles, Louisiana.

†Professor, Department of Mechanical Engineering. Member AIAA.

Introduction

In the design of turbine blade cooling passages, turbulence promoters (rib turbulators) often enhance the heat transfer. Periodic rib-turbulators are cast on two opposite walls of a straight or a serpentine rectangular channel. In a straight rib-roughened channel, the effects of the channel aspect ratio, the turbulators' configurations (such as rib height, spacing, and angle), the flow Reynolds number on the local heat transfer coefficient, and the pressure drop were reported by Han et al.[1–4] The angled ribs enhanced heat transfer more than the transverse ribs. Based on the law of the wall similarity, correlations for the heat transfer and friction were obtained.

In a serpentine rib-roughened channel, as shown in Fig. 1, in addition to the rib turbulators, the effects of the sharp 180-deg turns on the local heat transfer coefficient and the pressure drop are important. The local heat transfer coefficient in a two-pass square channel roughened by the transverse ribs was reported by Boyle.[5] With the naphthalene sublimination technique, the distributions of the local mass transfer coefficient in a two-pass square channel roughened by the transverse ribs and by the angled ribs were presented by Han et al.[6] and by Chandra et al.,[7] respectively. After the sharp 180-deg turn, in general, the mass transfer coefficients were higher than those before the turn.

In Refs. 6 and 7, emphasis was on determining the combined effects of the rib configuration and the sharp 180-deg turn on the detailed distributions of the local mass transfer coefficient in the before-turn and after-turn regions. The average mass transfer coefficients for the entire two-pass channel were not presented. Neither have the combined effects of the rib configuration and the sharp 180-deg turn on the distributions of the local and average pressure drops for the entire two-pass square channel been reported. The following questions remain: 1) in a two-pass channel, whether the angled ribs enhance heat transfer better than the transverse ribs and 2) whether the two-pass rib-roughened channel enhances heat transfer better than the first-pass rib-roughened channel.

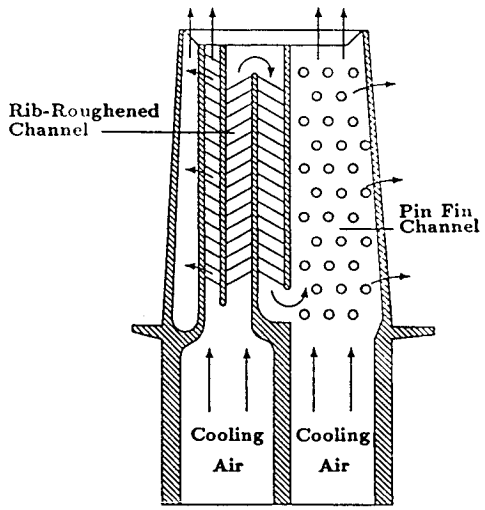

Fig. 1 Cooling concept of a modern turbine blade.

The objective of the present study was to investigate the combined effects of the sharp 180-deg turn and the rib configuration on the distributions of the local pressure drop and the mass transfer coefficient in two-pass square channels for Reynolds numbers from 15,000–60,000. A Plexiglas two-pass square channel was used for pressure drop measurements. A separate two-pass square channel fabricated of naphthalene-coated plates was used for mass transfer experiments. The square brass ribs were attached to the top and bottom surfaces of the two straight sections of the test channel so that the rib turbulators on opposite walls were parallel. The effect of the sharp 180-deg turn on the pressure drop and mass transfer was determined. Heat transfer performance for angled ribs and transverse ribs was compared for the first pass and for the two-pass channel. Additional information on the present investigation is in Chandra[8] and Han and Chandra.[9]

Experimental Program

Mass Transfer Test Channel

Figure 2a is a schematic of the test section for mass transfer experiments. The test section, made of aluminum, was a two-pass channel with a 2.54-cm (1-in.) square cross section. The gap at the tip of the divider wall (inner wall) also measured 2.54 cm (1 in.). To simulate actual turbine cooling passages, the length of each of the two straight sections of the test channel was 13 times the channel hydraulic diameter, and the thickness of the divider wall was 0.25 times the hydraulic diameter. The inside surfaces were coated with naphthalene in a casting process, against a highly polished stainless steel plate. Brass ribs (without naphthalene coating) with a 0.159-cm (0.063-in.) square cross section were glued periodically in-line on the naphthalene-coated top and bottom surfaces of the two straight sections of the test channel. The rib height-to-hydraulic diameter ratio was 0.063; the rib pitch-to-height ratio was 10; the rib angle-of-attack was 90 or 60 deg. No rib was placed in the turn region.

Mass Transfer Data Reduction and Uncertainty

A Starrett electronic depth gage with an accuracy of 0.0001 in./0.0001 mm determined the contours of all the naphthalene surfaces before a test run. The naphthalene plate, whose contour was to be measured, was mounted firmly on an x-y coordinate table. The data were recorded with a TI computer connected to the amplifier of the electronic depth gage through an A/D converter. The test section was then assembled for the mass transfer experiment. A typical run

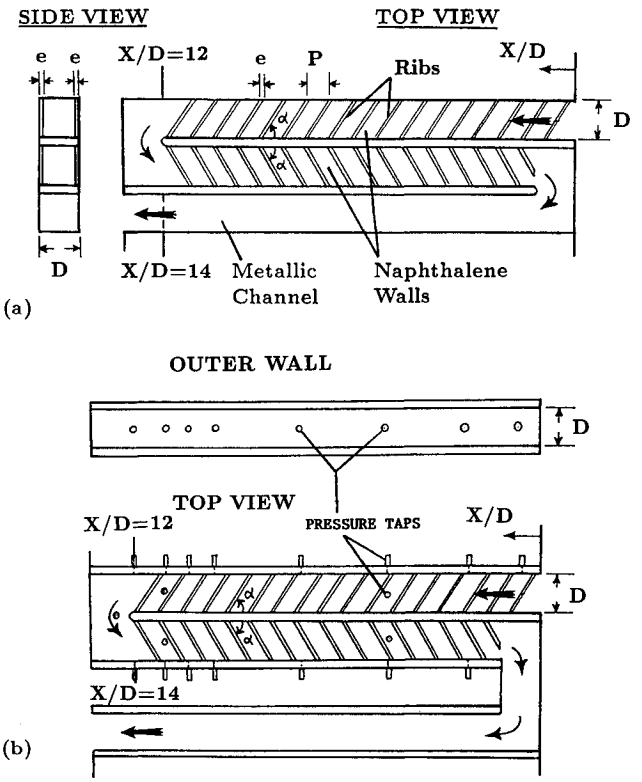

Fig. 2 Sketch of the test sections: a) mass transfer and b) pressure drop.

lasted about 30 min. After the test run, the contours of the naphthalene surfaces were measured and recorded again. From the corresponding before-run and after-run surface contours, the depth change ΔZ at each measurement station on the naphthalene surfaces was calculated. The mass transfer flux at the measurement point was evaluated as

$$\dot{m}'' = \rho_s \cdot \Delta Z/\Delta t \tag{1}$$

and the corresponding mass transfer coefficient at the same measurement point was then determined as

$$h_m = \dot{m}''/(\rho_w - \rho_b) \tag{2}$$

The local naphthalene vapor density ρ_w was calculated from the ideal gas law in conjunction with the measured naphthalene surface temperature and with the vapor pressure-temperature relationship for naphthalene developed by Sogin.[10] The bulk naphthalene vapor density (ρ_b) was the cumulative mass transferred from the naphthalene surfaces to the air stream divided by the air volumetric flow rate.

The local mass transfer coefficient was converted to the local Sherwood number as

$$Sh = h_m \cdot D/\tilde{D} = h_m \cdot D/(\nu/Sc) \tag{3}$$

where the Schmidt number for naphthalene was 2.5.[10] The local Sherwood number of the present study was normalized by the Sherwood number for fully developed turbulent flow in smooth circular tubes, correlated by McAdams as

$$Sh/Sh_o = Sh/[0.023Re^{0.8}Pr^{0.4}(Sc/Pr)^{0.4}] \tag{4}$$

where the heat and mass transfer analogy,[10] $Nu_o/Sh_o = (Pr/Sc)^{0.4}$, was employed. The maximum uncertainty in the Sherwood number was estimated to be less than 8% by the uncertainty estimation method of Kline and McClintock.[11]

Separate tests were conducted to determine the mass losses from the various naphthalene surfaces caused by natural convection when the ribs were being glued on the appropriate naphthalene surfaces and when the surface contours were being measured. The total mass loss by natural convection was no more than 4% of the total mass transfer during any test run. In calculating the local Sherwood numbers, these losses of mass from the various naphthalene surfaces were taken into account accordingly.[9]

Note that the boundary conditions on the naphthalene-coated channel walls with glued-on brass ribs (with surfaces from which no mass is transferred) in the current mass transfer experiments are analogous to the boundary conditions on the foil-heated channel walls with glued-on Bakelite ribs in Boyle's heat transfer experiments.[5] Boyle[5] found that the local heat transfer coefficients in channels with integral foil-ribs and glued-on Bakelite ribs were within 10% of each other. Based on Boyle's results, the use of brass ribs instead of naphthalene-coated ribs may result in an error of about 10% in the local mass transfer coefficients in the present study.

Pressure Drop Test Channel

Figure 2b is a schematic of the test section for pressure drop experiments. The internal geometry of the test section and the construction were similar to that of the mass transfer test section; the only difference was Plexiglas instead of aluminum for construction. Brass ribs were glued onto the top and bottom surfaces of the two straight sections of the test channel. The ribs on the top surfaces were parallel to those on the bottom surfaces of the test channel. The rib height-to-hydraulic diameter ratio was 0.063 or 0.094; the rib pitch-to-height ratio was 10 or 20; the rib angle-of-attack was 90, 60, or 45 deg. No rib was placed in the turn region. In the two-pass channel, 15 pressure taps along the outer smooth wall and 5 along the top ribbed wall were used for the static pressure drop measurements, as shown in Fig. 2b. The pressure drop across the test section was measured by a Dywer microtector, with an accuracy up to 0.025-mm (0.001-in.) of water. The pressure drop of the present study was based on the adiabatic conditions (test without heating).

Friction Factor and Loss Coefficient

During the experiments, the magnitude of the pressure drop was almost the same on the smooth side and the ribbed side walls. Therefore, the pressure drop and the friction factor calculations were on the basis of the average values. The distributions of the local pressure drop in the two-pass channel were normalized by the fluid dynamic pressure as

$$(P_x - P_i)/[(1/2)\rho V^2] \tag{5}$$

On the basis of the normalized pressure distribution results, the channel was divided into four regions: the entrance region ($X/D = 0$–4.69), the fully developed before-turn region ($X/D = 4.69$–10.94), the turn region ($X/D = 10.94$–18.8), and the fully developed after-turn region ($X/D = 18.8$–23.8). The following equation was used to calculate the friction factors in the fully developed before- and after-turn regions of the channel:

$$\bar{f}_{bt}\,(\text{or}\,\bar{f}_{at}) = \Delta P/\{4(\Delta L/D)[G^2/(2\rho g_c)]\} \tag{6}$$

The loss coefficient caused by sudden contraction at the entrance ($X/D = 0$–4.69) and the loss coefficient for the turn region ($X/D = 10.94$–18.8) were calculated by the following relation:

$$K_c\,(\text{or}\,K_t) = \Delta P/[G^2/(2\rho g_c)] \tag{7}$$

The maximum uncertainty in the friction factor was estimated to be less than 8%.

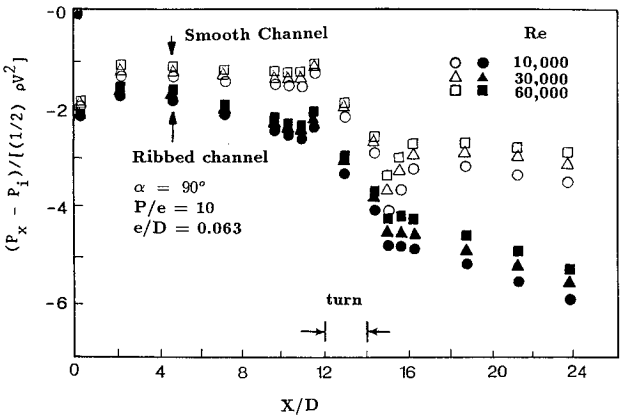

Fig. 3 Effect of Reynolds number on normalized pressure drop.

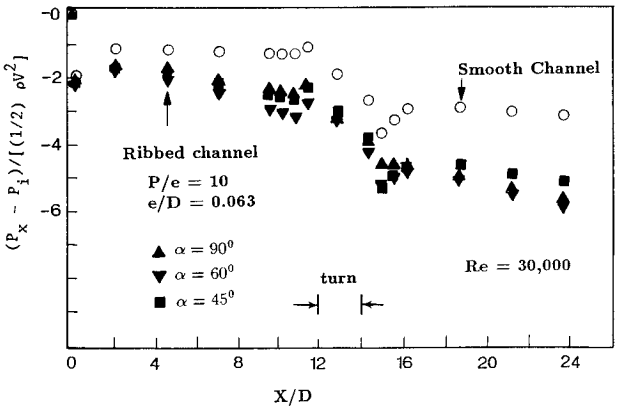

Fig. 4 Effect of rib angle on normalized pressure drop.

Experimental Results and Discussion

Local Pressure Drop

The detailed raw data for all test runs are in Chandra[8] and Han and Chandra.[9] Only the most representative results are presented here. The local pressure drop results are presented as the axial distributions of a dimensionless pressure drop, as shown in Eq. (5).

Effect of Reynolds Number

Typical results to demonstrate the effect of Reynolds number on the dimensionless local pressure drop in a two-pass square channel are shown in Fig. 3 for $e/D = 0.063$, $P/e = 10$, and $\alpha = 90$ deg. The results in the same channel with smooth surfaces are included for comparison. The dimensionless pressur drop has the same trend for all Reynolds number and decreases with increasing Reynolds number. The pressure drops sharply at the sudden contraction entrance ($X/D \simeq 0.5$) of the channel in all Reynolds numbers. The pressure rises near $X/D = 2$ and drops linearly until before the turn ($X/D \simeq 11$). The pressure then rises slightly in the vicinity of the upstream corner of the turn ($X/D \simeq 11.5$). There is a rapid pressure drop in and just after the turn region ($X/X \simeq 11.5$–15). The pressure then increases slightly ($X/D \simeq 16$). There is a pressure drop towards the end of the second straight section of the channel ($X/D \simeq 16$–24). In the smooth channel, the pressure drop is caused primarily by the sharp 180-deg turn. In the ribbed channel, the pressure drop is caused by both the sharp turn and the rib turbulators on the two straight sections of the channel.

Effect of Rib Configuration

Typical results to illustrate the effect of rib angle on the dimensionless local pressure drop are in Fig. 4 for $P/e = 10$, $e/D = 0.063$, and $Re = 30{,}000$. The smooth channel results are included for comparison. The distributions of the dimensionless local pressure drop show the same trend as the smooth channel, for all rib angles. Again, in the ribbed channel, the pressure drop is caused by both the sharp 180-deg turn and the ribs on the two straight sections of the channel.

Friction Factor and Loss Coefficient

The results for fully developed friction factors vs Reynolds number for different rib configurations are shown in Fig. 5. For the smooth channel, the friction factor in the before-turn region is about 6% lower than that the Blasius equation; the friction factor in the after-turn region is about 100% higher. For the ribbed channel, the friction factor approaches an approximately constant value as the Reynolds number increases; the friction factor increases with rib size and decreases with rib spacing; the friction factor, with $\alpha = 60$ deg is higher than any other rib angle-of-attack. Note that the friction factor in the after-turn region is higher than the corresponding before-turn region, except in cases with $\alpha = 60$ deg and $\alpha = 45$ deg, in which $\bar{f}_{at}$ is lower than their respective values for $\bar{f}_{bt}$.

The results for loss coefficients vs Reynolds number for different rib configurations are shown in Fig. 6. The loss coefficient, in general, decreases with increasing Reynolds number. Both loss coefficients for the ribbed channel are higher than that for the smooth channel. For $P/e = 10$, the contraction loss coefficient (K_c), with $\alpha = 90$ deg is lower than that with $\alpha = 60$ deg and $\alpha = 45$ deg. However, the turning loss coefficient (K_t), with $\alpha = 90$ deg is higher than that with $\alpha = 60$ deg and $\alpha = 45$ deg.

Correlations

The two fully developed friction factors, $\bar{f}_{bt}$ and $\bar{f}_{at}$, and the two loss coefficients, K_c and K_t, were correlated by a single equation of the following form:

$$\bar{f}_{bt}(\text{or } \bar{f}_{at}, K_c, K_t) = a(Re)^b[(P/e)/10]^c[(e/D)/0.063]^m(\alpha/90°)^n \quad (8)$$

where the coefficients a, b, c, m, and n are given in Table 1. The deviations in Eq. (8) from the test data are $\pm 7\%$, $\pm 10\%$ ($\pm 8\%$ for 95% data points), $\pm 5.5\%$, and $\pm 6.6\%$, respectively, for $\bar{f}_{bt}$, $\bar{f}_{at}$, K_c, and K_t. Note that results for the friction factor in the before-turn region, $\bar{f}_{bt}$, agree with those published in Ref. 2.

Mass Transfer Coefficient

Local Sherwood Number Ratio

The local Sherwood number ratios at two rib pitches before the turn, in the turn, and at two rib pitches after the turn are shown in Fig. 7 for the smooth channel and for the ribbed channel, with $P/e = 10$, $e/D = 0.063$, and $\alpha = 90$ deg (and $\alpha = 60$ deg), respectively. For the smooth channel, the Sh/Sh_o ratio before the turn, in the turn, and after the turn is about 1–1.1, 1.5–2.0, and 2.0–2.5, respectively. For the ribbed channel, the local Sherwood number ratios are higher than the corresponding smooth channel values because of turbulence created by ribs. Before the turn, the ribbed-wall Sh/Sh_o ratio for $\alpha = 90$ deg is relatively uniform in the spanwise direction; the ribbed-wall Sh/Sh_o ratio for $\alpha = 60$ deg decreases from the outer wall towards the inner wall because of the secondary flow induced by the rib axes (rib angles). After the turn, the ribbed-wall Sh/Sh_o ratio for both $\alpha = 90$ deg and $\alpha = 60$ deg decreases from the outer to the inner wall because of the main flow turning from the outer wall towards the inner wall.

Effect of Reynolds Number and Rib Angle

In this section, the Sherwood number ratios were based on the average of the local Sherwood number ratios between every two adjacent ribs. At the entrance ($X/D = 0.5$–2.0), before the turn ($X/D = 7$–8 and 9–12), after the turn ($X/D = 14$–17 and 18–19), and at the end of the second straight section ($X/D = 24$–25.5), the Sherwood number ratios on the ribbed-wall were based on the average of 24 measure-

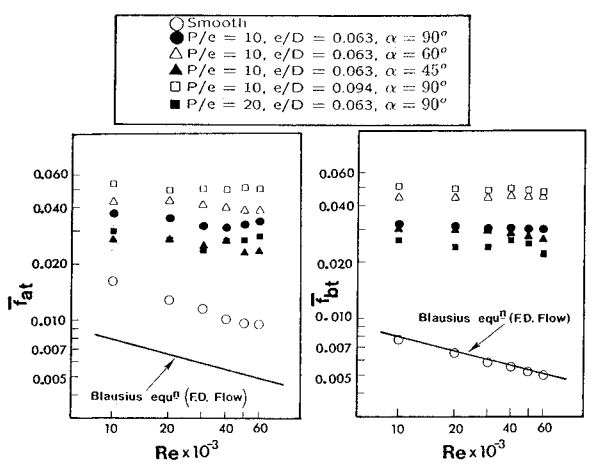

Fig. 5 Fully developed friction factors vs Reynolds number.

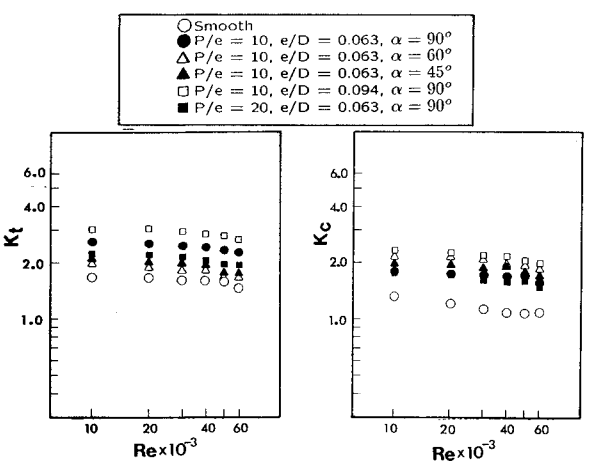

Fig. 6 Loss coefficients vs Reynolds number.

Table 1 Coefficients a, b, c, m, and n in Eq. (8)

Region/factor	a	b	c	m	n if $\alpha \geq 60$ deg	n if $\alpha < 60$ deg
$\bar{f}_{bt}$	0.0432	−0.034	−0.342	1.173	−0.865	0.105
$\bar{f}_{at}$	0.0476	−0.032	−0.37	0.99	−0.447	0.46
K_c	2.54	−0.04	−0.05	0.595	−0.435	−0.12
K_t	3.25	−0.029	−0.215	0.42	0.75	0.32

ment points every rib pitch (a matrix of 8 points in streamwise direction by 3 points in spanwise direction between two adjacent ribs, as shown in Fig. 7). At the rest of X/D ratios, the Sherwood number ratios on the ribbed-wall were based on the average of 3 measurement points every rib pitch (3 points in spanwise direction at the middle of two adjacent ribs measured from rib axes).

Typical results showing the effect of Reynolds number on the Sherwood number ratio on the rib-side-wall are in Fig. 8 for $e/D = 0.063$, $P/e = 10$, and $\alpha = 90$ deg. The results indicate that the Sherwood number ratios have the same trends for all Reynolds numbers and decreases with increasing Reynolds number. In the entrance section, the Sherwood number ratios decrease with increasing axial distance until before the turn ($X/D \simeq 11.5$). At $X/D = 12$–14, the Sherwood number ratios are relatively low because there are no ribs in the turn region. The Sherwood number ratios reach the peak values after the sharp turn ($X/D \simeq 15$) and then decrease with further increasing axial distance towards the end of the second section of the channel. For more uniform mass (heat) transfer distribution, ribs should be placed in the turn region, also.

Typical results showing the effect of rib angle on the Sherwood number ratio are in Fig. 9 for $P/e = 10$, $e/D = 0.063$, and $Re = 30{,}000$. The four-sided, smooth channel data are included for comparison. The Sherwood number ratio on the rib-side-wall for $\alpha = 90$ deg shows the same trend as that of the smooth channel, except that the former is higher. The distributions of the Sherwood number ratio for $\alpha = 60$ deg behave differently from that of $\alpha = 90$ deg. For $\alpha = 60$ deg, in the entrance section, the Sherwood number ratio decreases first and then slightly increases until before the turn because of the effect of the rib angle. The Sherwood number ratios right after the turn ($X/D \simeq 14$–17) are lower than those before the turn, and then increase toward the end of the second straight section of the channel, because of the complex influence between the rib angle and the sharp 180-deg turn.

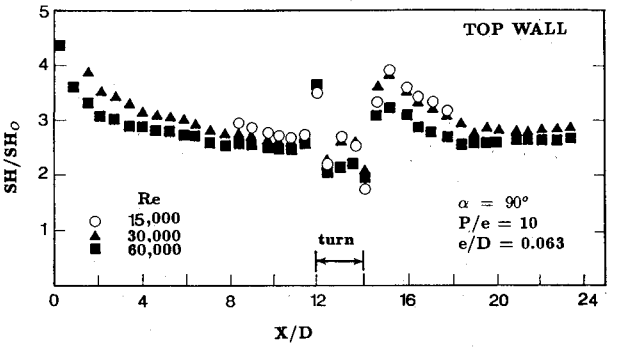

Fig. 8 Effect of Reynolds number on rib-side-wall Sherwood number ratio.

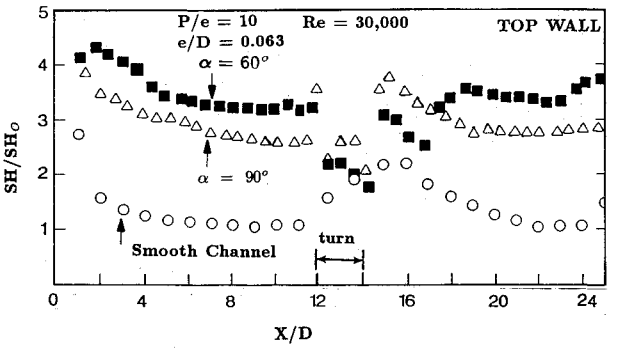

Fig. 9 Effect of rib angle on rib-side-wall Sherwood number ratio.

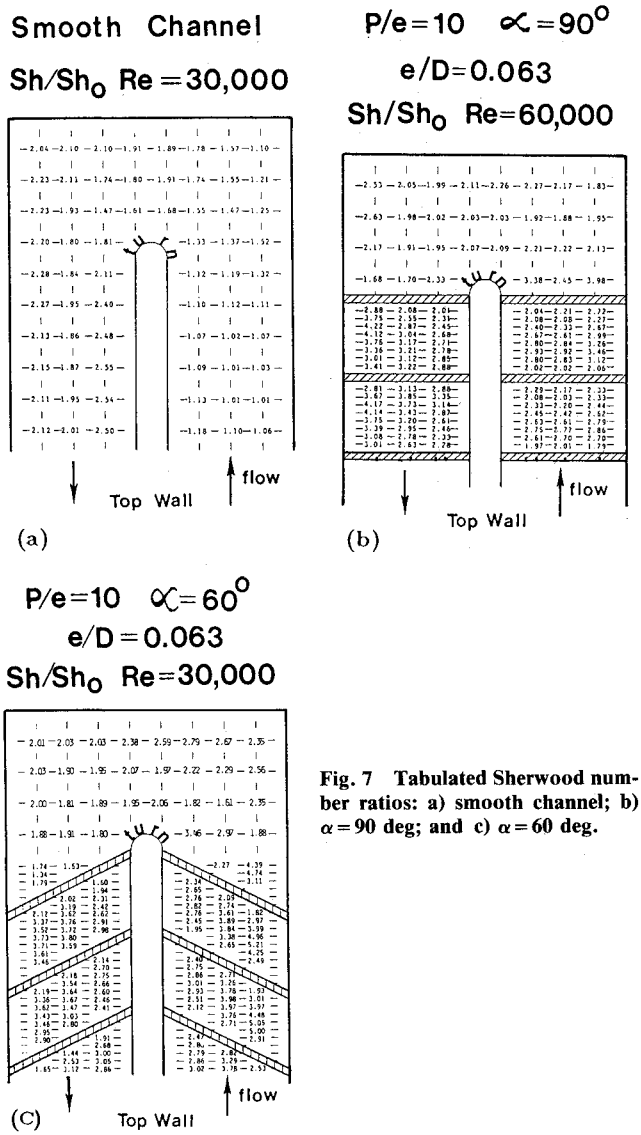

Fig. 7 Tabulated Sherwood number ratios: a) smooth channel; b) $\alpha = 90$ deg; and c) $\alpha = 60$ deg.

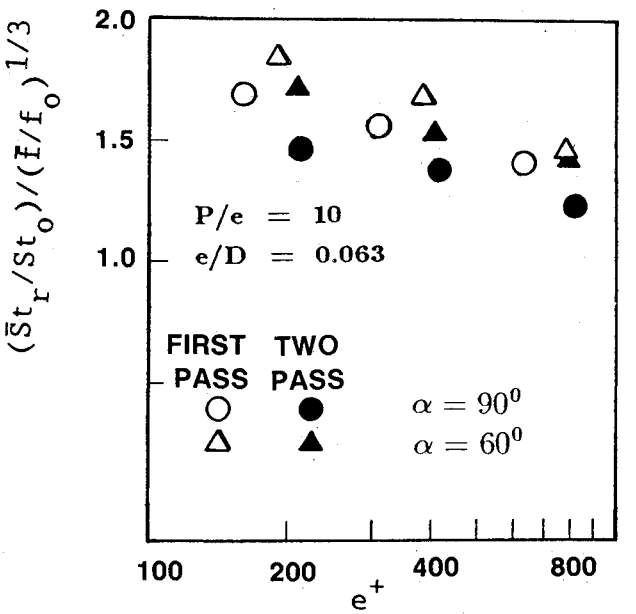

Fig. 10 Enhanced heat transfer comparison for a constant pumping power.

Heat Transfer Performance Comparison

One of the performance evaluation methods was a comparison of the increased heat transfer on the ribbed wall, $(\bar{St}_r/St_o)/(\bar{f}/f_o)^{1/3}$, for the same pumping power, as discussed in Ref. 2. Sherwood numbers of the present study were converted into Nusselt numbers by the heat and mass transfer analogy; Nusselt numbers were changed to Stanton numbers accordingly.

Typical results of the effect of rib angle on the increased heat transfer for the same pumping power are shown in Fig. 10 for the first pass ($X/D = 4.56$–11.63) and the two-pass ($X/D = 4.56$–23.31) channels, respectively. The ratio of the enhanced heat transfer to the increased friction factor decreases with increasing roughness Reynolds number e^+ (i.e., larger rib height or higher Reynolds number). There is higher heat transfer enhancement with the angled ribs ($\alpha = 60$ deg) than with the transverse ribs ($\alpha = 90$ deg) in the first pass of the two-pass channel. The increase in heat transfer performance is reduced for the two-pass channel because the friction factors are much higher than those in the first pass, and the heat transfer coefficients are only slightly higher than those in the first pass, as discussed in the previous section.

Concluding Remarks

The combined effects of the rib angle and the sharp 180-deg turn on the pressure drop and mass transfer characteristics in a two-pass square channel have been investigated. The main findings are:

1) The ratio of the enhanced heat transfer to the increased pressure loss in the two-pass channel is slightly lower than that in the first-pass channel.

2) In the first-pass channel, the enhanced heat transfer with angled ribs is higher than that with the transverse ribs for the same pumping power. The performance improvement of the angled ribs is reduced in the two-pass channel.

3) Correlations for the fully developed friction factors and the loss coefficients are obtained for the first-pass and the two-pass channels with rib turbulators.

Note that, in real turbine cooling passages, heat is transferred from the ribs and from the exposed surfaces of the channel walls. The present mass transfer coefficients were obtained without including mass transfer from the ribs.

Acknowledgment

This work was funded in part by the NASA Lewis Research Center, through Contract NAS 3-24227.

References

[1]Han, J. C., "Heat Transfer and Friction in Channels with Two Opposite Rib-Roughened Walls," *ASME Journal of Heat Transfer*, Vol. 106, Nov. 1984, pp. 774–781.

[2]Han, J. C., Park, J. S., and Lei, C. K., "Heat Transfer Enhancement in Channels with Turbulence Promoters," *ASME Journal of Engineering for Gas Turbines and Power*, Vol. 107, July 1985, pp. 628–635.

[3]Han, J. C. and Park, J. S., "Developing Heat Transfer in Rectangular Channels with Rib Turbulators," *International Journal of Heat Mass Transfer*, Vol. 31, Jan. 1988, pp. 183–195.

[4]Han, J. C., "Heat Transfer and Friction Characteristics in Rectangular Channels with Rib Turbulators," *ASME Journal of Heat Transfer*, Vol. 110, May 1988, pp. 321–328.

[5]Boyle, R. J., "Heat Transfer in Serpentine Passages with Turbulence Promoters," American Society of Mechanical Engineers Paper 84-HT-24, 1984.

[6]Han, J. C., Chandra, P. R., and Lau, S. C., "Local Heat/Mass Transfer Distributions Around Sharp 180 Degree Turns in Two-Pass Smooth and Rib-Roughened Channels," *ASME Journal of Heat Transfer*, Vol. 110, Feb. 1988, pp. 91–98.

[7]Chandra, P. R., Han, J. C., and Lau, S. C., "Effect of Rib Angle on Local Heat/Mass Transfer Distribution in a Two-Pass Rib-Roughened Channel," *ASME Journal of Turbomachinery*, Vol. 110, April 1988, pp. 233–241.

[8]Chandra, P. R., "A Study of Local Heat/Mass Transfer Distribution in Multipass Channels for Turbine Blade Cooling," Ph.D. Thesis, Texas A&M Univ., College Station, TX, Aug. 1987.

[9]Han, J. C. and Chandra, P. R., "Local Heat/Mass Transfer and Pressure Drop in a Two-Pass Rib-Roughened Channel for Turbine Airfoil Cooling," NASA Lewis Research Center, OH, NASA CR-179635; also AVSCOM-TR-87-C-14, Sept. 1987, pp. 1–166.

[10]Sogin, H. H., "Sublimation from Disks to Air Streams Flowing Normal to Their Surfaces," *Transactions of the ASME*, Vol. 80, Jan. 1958, pp. 61–69.

[11]Kline, S. J. and McClintock, F. A., "Describing Uncertainties in Single-Sample Experiments," *Mechanical Engineering*, Vol. 75, Jan. 1953, pp. 3–8.